Inter-Research Science Publisher

Endangered Species Research
Volume 60:esr01505

Published June 4, 2026
https://doi.org/10.3354/esr01505

OPEN ACCESS

Body condition differs among social clusters and across years in endangered false killer whales in Hawai'i

Jens J. Currie[1,2,✉], Brian Stirling[1], Grace Olson[1], Martin van Aswegen[2], Lewis Evans [2], Stephanie H. Stack[1,3], Nozomi Kobayashi[4,5], Keiichi Ueda[4,5], Suguru Higa[5], William Gough[2], Fabien Vivier[2], Liah McPherson[2], Kyleigh Fertitta[2], Lars Bejder[2]

[1]Pacific Whale Foundation, Wailuku, HI 96793, USA
[2]Marine Mammal Research Program, Hawai'i Institute of Marine Biology, University of Hawai'i at Mānoa, HI 96744, USA
[3]Southern Ocean Persistent Organic Pollutants Program, School of Environment and Science, Griffith University, Nathan, QLD 4111, Australia
[4]Okinawa Churashima Research Institute, Okinawa Churashima Foundation, 888 Ishikawa, Motobu, Okinawa 905-0206, Japan
[5]Okinawa Churaumi Aquarium, Okinawa Churashima Foundation, 424 Ishikawa, Motobu, Okinawa 905-0206, Japan

ABSTRACT: Body condition is a critical indicator of health and nutritional status in cetaceans, particularly for small, endangered populations facing ecological stressors. We used aerial photogrammetry to evaluate body size and condition of the endangered false killer whale *Pseudorca crassidens* population resident in the main Hawaiian Islands. From 2019 to 2025, 68 individuals were assessed across 142 photogrammetric measurements. Relative body width declined with age class, particularly across the mid-body region, indicating early-life lipid accumulation followed by increased energetic demands in adulthood. Photogrammetric volume estimates were validated against 3D-scanned individuals, providing estimates within 3% of scanned volumes. Standardized major axis regression revealed significant differences in the body length—volume relationship across social clusters. Body condition index (BCI) varied across years, with the lowest values in 2020, coinciding with the largest single-year population decline and record sea surface temperatures from a marine heatwave, suggesting that environmental stressors may have contributed to reduced body condition during this period. Individual-level trajectories further highlighted substantial fluctuations in BCI, including one case of 28% estimated body mass loss over a 2.5 mo period, and pronounced variability within one cluster, potentially reflecting higher energetic costs and nutritional stress associated with broader ranging behavior. These findings underscore the influence of spatial ecology and local prey availability on the health of this declining population, while providing a foundation for long-term monitoring of the energetic stressors shaping their viability.

KEY WORDS: False killer whale · Body condition · Photogrammetry · Social clusters · Hawai'i · Conservation

HŌ'ULU'ULU MANA'O: O ke kino he mea e hō'ike i ke ola kūpono a me ka 'ai kūpono o nā koholā a no nā koholā li'ili'i, i kokoke o ka make loa o ko lākou lāhui ma muli o nā hewa o ka 'āina. Ua ho'ohana kākou i ka pa'i ki'i mai ka lani e nānā i ka nui o ke kino a me ke ola o nā koholā 'ele'ele (FKW - Pseudorca crassidens) i noho ai ma ka pae 'āina 'o Hawai'i. Mai 2019—2025, ua nānā 'ia he 68 mau nai'a 'ele'ele mai 142 pa'i ki'i. Ua 'emi mai ka nui o ka laulā i ka hui o nā makahiki i ola, me ka 'emi nui ma ka waena o ka wahi kino. Hō'ike kēia i ka ho'omomona 'ana i ka wā 'ōpio a laila ka makemake'ia o ka ikehu ke ulu a'e i makua. I ka nānā pono i kea māu ki'i, hō'ike 'ia ka pono o kēia

✉Corresponding author: jenscurrie@pacificwhale.org

Publisher: Inter-Research · www.int-res.com

ʻike me ka 3-D lolelole o nā naiʻa ʻeleʻele. Kūpono kēia ʻike me ka 3% o nā kiʻi a pau. Ua hōʻike ka hōʻemi ʻana o ka nui o ke kino ʻawelika i ka ʻokoʻa o ka lōʻihi o ke kino. Ka pilina o ka nui o ke kino i nā hui pū o na koholā ʻeleʻele. Ua ʻokoʻa ka BCI i nā makahiki like ʻole. Ma ka makahiki 2020 ua lilo ai ka makahiki me ka ʻemi loa o nā koholā ʻeleʻele a me ka makahiki me ke kai i wela loa. Maliʻa paha, ka hewa o ka ʻāina i hōʻeha ʻai i ke koholā ʻeleʻele a me ka nui o ke kino o ke koholā ʻeleʻele i kēia wā. Hōʻike ke ala ola o nā koholā ʻeleʻele i ka luli o ka BCI. I hoʻokahi o lākou, ua hōʻemi kona kino i 28% i he 2.5 mau mahina. I hoʻokahi hui o nā koholā ʻeleʻele, ua luli ko lākou BCI, maliʻa paha ma muli o ka hoʻonui o ka ikehu a me ka ʻai hewa me nā hana aʻe. O ka hopena o kēia ʻimi naʻauao o ke koʻikoʻi o ke kaʻawale o nā iʻa a me ka nui o ka pio ʻai i hōʻemi ana i ka lāhui koholā ʻeleʻele. I ka manawa like e hāʻawi i ke kāhua no ka nānā loa i ka hewa i nā ikehu.

1. INTRODUCTION

The Main Hawaiian Islands (MHI) insular population of false killer whales *Pseudorca crassidens* is listed as endangered under the US Endangered Species Act (NMFS 2012) and has experienced an approximately 3.5% yr^{-1} decline over the last decade, with the population estimated at 139 individuals (95% CI: 114–162) in 2022 (Badger et al. 2025). While the energetic needs of this population are unknown, studies of false killer whales in human care suggest daily intake requirements range between 2.9 and 6.1% of body weight (Kastelein et al. 2000). Like other odontocetes, false killer whales likely exhibit elevated energetic demands associated with thermoregulation (Costa & Williams 1999) and a carnivorous diet (Williams et al. 2001). These factors, combined with potential ecological constraints, suggest that even modest fluctuations in prey availability could impair their ability to meet energetic demands, which, in turn, can influence body condition and survival (Stewart et al. 2021a, Rojano-Doñate et al. 2024). In some cases, reduced energy intake due to declining prey size and dispersion can lead to population collapse, as demonstrated in harbor porpoises *Phocoena phocoena* (Gallagher et al. 2022). As such, monitoring the body condition of free-ranging cetaceans can help us to understand the impacts of ecosystem changes that affect the trophic dynamics in a particular region (Durban et al. 2021, Stewart et al. 2021a, Kotik et al. 2023). Nutrient levels are generally considered low in the MHI, with the highest productivity occurring nearshore (Gilmartin & Revelante 1974), which congregates large prey species targeted by false killer whales such as yellowfin tuna *Thunnus albacares*, broadbill swordfish *Xiphias gladius*, wahoo 'ono' *Acanthocybium solandri*, and mahimahi *Coryphaena hippurus* (Baird 2009, Oleson et al. 2010).

Here, we systematically evaluate changes in body condition among individuals and across social clusters of false killer whales over a 7 yr period. Specifically, we compare body volume across social clusters, track individual fluctuations over time, and assess patterns consistent with nutritional stress.

There are 3 populations of false killer whales found in the Hawaiian archipelago. The MHI insular false killer whale population is genetically and socially distinct from the pelagic and Northwestern Hawaiian Islands populations (Chivers et al. 2007, 2010, Baird et al. 2008, Martien et al. 2014). Social network analyses have identified 4 long-term social clusters within the MHI insular population, characterized by persistent associations among individuals that include both kin and non-kin relationships (Mahaffy et al. 2023). These proportions are based on the number of distinct individuals seen on ≥5 d over a 23 yr period and therefore reflect estimates that are biased toward individuals that were more readily identifiable and repeatedly encountered rather than true cluster membership sizes. Each cluster broadly shares an overall range and general habitat-use patterns throughout the MHI, with evidence of distinct fine-scale space use reflected in cluster-level core areas (Mahaffy et al. 2023, Kratofil et al. preprint doi:10.64898/2026.02.06.704493). High-use areas of Clusters 1, 3, and 4 overlap off Molokaʻi, with Clusters 1 and 3 exhibiting the broadest high-use areas that span both Maui Nui and adjacent channel waters to varying extents, whereas Clusters 2 and 4 have more restricted and spatially distinct core areas, centered primarily in the ʻAlenuihāhā Channel and Maui Nui to Kaiwi Channel waters, respectively (Baird et al. 2012, 2019, 2023, Silva 2013). Cluster 1 shows one of the largest core-area spatial extents, suggesting a wide-ranging spatial pattern. (Baird et al. 2023). Variation in pollutant ratios and stable isotope values among clusters is also consistent with these differences in space use and foraging behavior, indicating cluster-level variation in exposure pathways and trophic ecology (Baird et al. 2015, Kratofil et al. 2020, Harnish et al. 2024). However, the extent to which spatial ecology or ranging behavior translates into

differences in body condition or energetic status remains unresolved.

Locomotion is energetically costly for marine mammals, particularly at sustained swim speeds (Costa & Williams 1999, Allen et al. 2022, Williams & Davis 2024), and this suggests a plausible link between ranging behavior and energetic demands, with potential implications for body condition. Part of the known diet of the MHI insular population comprises large pelagic species such as yellowfin tuna and mahimahi, which are also targeted by Hawai'i's commercial fisheries, resulting in direct competition for prey resources (Oleson et al. 2010) and documented fisheries interactions that vary among social clusters (Baird et al. 2015, Stack et al. 2019, Harnish et al. 2024). Clusters 1 and 3 exhibit the highest rates of fisheries interactions (28.7 and 38.2% of individuals, respectively), with multiple individuals showing evidence of repeated interactions acquired on different occasions, beginning as early as 2 yr of age (Harnish et al. 2024). Several key prey species, including yellowfin tuna, have declined significantly over the past century (Shomura 1987, Sibert et al. 2006), which may further intensify competition between false killer whales and fisheries. Furthermore, the average individual weight of pelagic fish species in Hawai'i has declined relative to historical values, indicating a reduction in body size over time (WPRFMC 2022). For example, the average weight of mahimahi in 2022 was 9.0 lbs (~4.1 kg), a 27% decrease from the 2013–2017 average of 12.4 lbs (~5.6 kg), while the average weight of wahoo declined to 35.0 lbs (~15.9 kg) in 2022, a 9% decrease from the 2013–2017 average of 38.4 lbs (~17.4 kg) (WPRFMC 2022).

Given these energetic constraints and environmental pressures, evaluating metrics of individual and population-level health is particularly important for this endangered false killer whale population, with body condition providing a valuable indicator of physiological status. Photogrammetry has long been used to infer cetacean health, and recent advances in unoccupied aerial systems-(UAS)-based imaging have improved the accuracy of individual morphometric assessments (Bradford et al. 2012, Christiansen et al. 2016, Durban et al. 2016, Currie et al. 2021, Vivier et al. 2023, van Aswegen et al. 2025b). UAS-based methods can be used to quantify daily fluctuations in body condition of small odontocetes (Currie et al. 2021), providing a noninvasive means of assessing whether individuals are experiencing nutritional stress. Nutritional stress can impair growth, reproduction, and immune function (Williams et al. 2013, Lundin et al. 2016, Wasser et al. 2017, Raverty et al. 2020, Currie et al. 2021), with consequences for individual fitness and population viability (Serres et al. 2024). A detailed understanding of nutritional stress and its cascading health effects is critical for developing effective conservation and management strategies that address the impacts of ecological disruption on wildlife populations (Pirotta et al. 2018, 2019, Booth et al. 2020, Keen et al. 2021).

Given that even short-term reductions in food intake can result in rapid declines in body mass and blubber thickness (Kastelein et al. 2019, Currie et al. 2021), measures of body condition provide a sensitive proxy of recent foraging success and nutritional status. For example, harbor porpoises lost up to 5% of body mass and 3 mm of blubber in a single 24 h near-fasting period (Kastelein et al. 2019). These changes occur primarily within metabolically active inner blubber layers and are associated with reductions in adipocyte size and number (Koopman et al. 2002), highlighting the responsiveness of body condition to short-term energetic shortfalls.

In this study, we first validated UAS photogrammetry for false killer whales by ground-truthing volume estimates against known measurements from animals under human care, providing methodological confidence. We then applied this technique to the MHI insular population to assess body condition in 3 of the 4 social clusters, compare body condition index (BCI) across clusters, quantify individual-level fluctuations over time, and evaluate patterns that may indicate nutritional stress.

2. MATERIALS AND METHODS

2.1. Data collection

High-resolution aerial videos (3840 × 2160 pixel) and dorsal fin photo-identification images, used to distinguish individuals based on unique fin markings (Würsig & Würsig 1977), were collected simultaneously for MHI insular false killer whales between 2019 and 2025 in waters extending up to 55 km (~30 nautical miles) from Maui Nui, including Maui, Kahoʻolawe, Molokaʻi, and Lānaʻi (Fig. 1). Data were acquired using a DJI Inspire 2 quadcopter equipped with either a Zenmuse X7 gimbal camera and a 35 mm *f*/2.8 LS ASPH lens or a Zenmuse X5S gimbal camera and a 25 mm *f*/1.8 lens. UAS calibration and the integration of an externally mounted laser altimeter followed protocols described by Dawson et al. (2017). The UAS was hand-launched and recovered from 2 research vessels: an 8 m fiberglass catamaran with twin 150 HP outboards, and a 9.1 m aluminum catamaran with twin 250 HP outboards. During

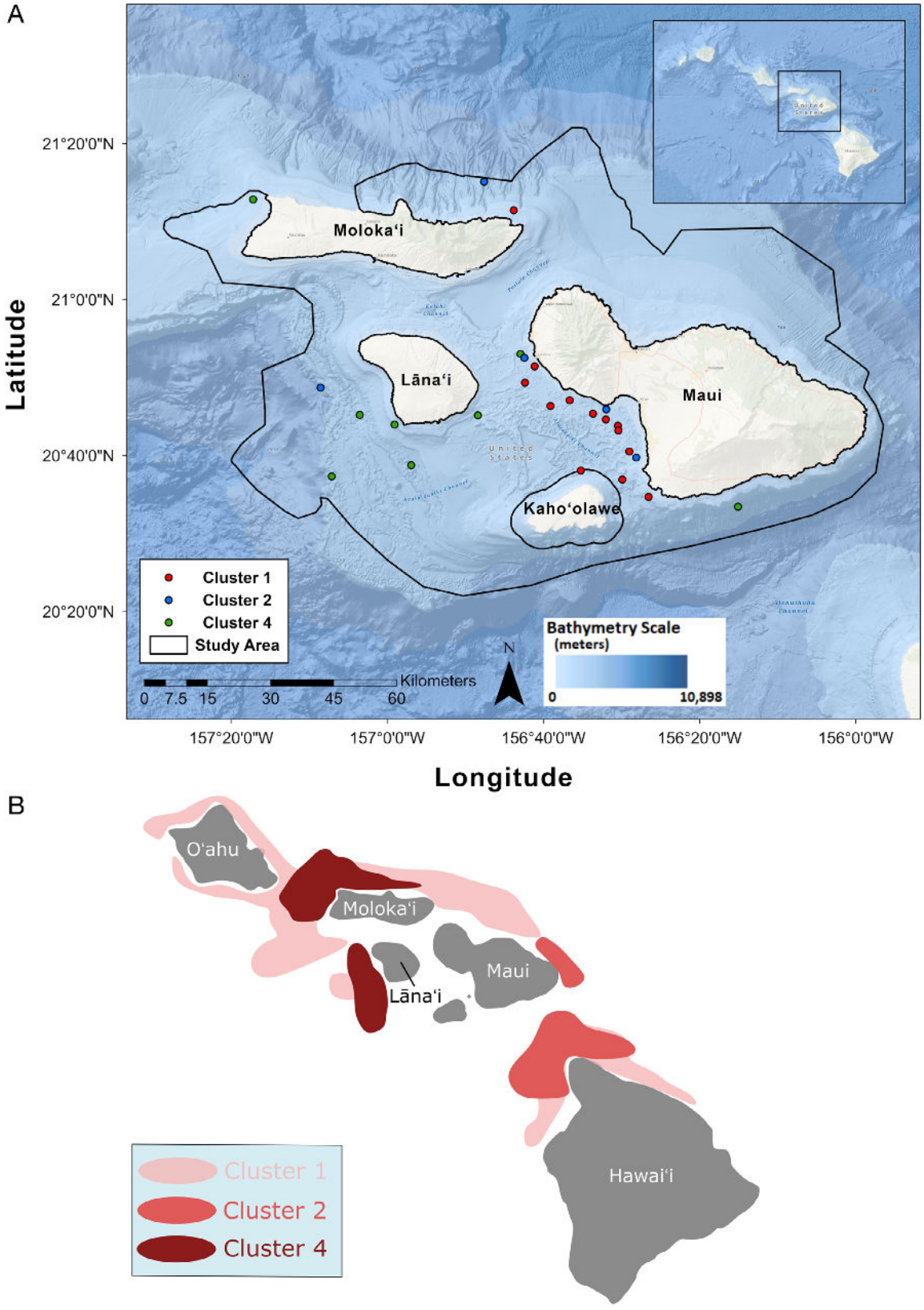

Fig. 1. (A) Spatial distribution of main Hawaiian Islands (MHI) insular false killer whale sightings with associated unoccupied aerial systems (UAS) photogrammetry from 2019 to 2025 across Maui Nui, Hawai'i. (B) High-use areas of the 3 insular false killer whale social clusters documented around the main Hawaiian Islands, adapted from Baird et al. (2023). High-use areas are based on telemetry data to provide context for potential ecological differences among clusters. Cluster 3 was not encountered in this study

sampling, the UAS was flown at an altitude of 15–35 m above the focal animal, with altitude recorded by an externally mounted altimeter at a frequency of 20 Hz. Previous validation using the same laser altimeter configuration demonstrated no systematic effect of altitude on measurement accuracy, with a mean (±SE) difference of 0.1 ± 1.3% between physical and UAS-derived total length measurements across altitudes of 16–50 m, indicating minimal altitude-related scaling or altimeter-associated error within the 15–35 m range used here (Vivier et al. 2023)

Data from each system were imported and processed in R (R Core Team 2025) following standard UAS photogrammetry workflows (Dawson et al. 2017), with modifications described here. Time synchronization between the UAS and laser altimeter data sets was achieved by aligning the first instance where the ascent rate exceeded 2 m s^{-1} in both systems, which occurs within the first 2–5 s of flight before animals are measured. To ensure data quality, laser altimeter measurements were discarded when the difference from the UAS internal altimeter exceeded 10 m and/or the absolute sum of aircraft pitch and roll exceeded 11°. Measurements sampled at 20 Hz were averaged at 1 Hz intervals. Altitude above sea level (ASL) was then calculated using the following equation and used to calibrate image scaling during photogrammetric analysis:

$$\text{ASL} = \cos(\text{pitch}) \times \cos(\text{roll}) \times \text{laser altimeter distance} \quad (1)$$

To maximize data collected from each encounter, including individuals that surfaced only once under the drone, missing values were replaced using the nearest valid measurement within a 2 s window, as drone height varied minimally over this interval. If no valid data were available within this range, the corresponding timestamps were excluded from consideration for video frame extraction.

Social cluster assignments were determined by matching dorsal fin photo-identification collected in the field, in conjunction with each UAS measurement, to the individual social cluster membership designations from Mahaffy et al. (2023).

2.2. Morphometrics

2.2.1. Total body length and width

Due to the steep surfacing angles and frequent arching during surfacing in false killer whales, a single image rarely provided an accurate measurement of total body length or width across the entire body. To address this limitation, and following methods adapted from Kotik et al. (2023), we obtained measurements from 2 sequential images during a surfacing period: a surfacing image and a diving image (Fig. 2). To account for the rapid change in shape of false killer whales and improve the precision of volumetric calculations, the body was divided into 22 segments, each representing approximately 4.5% of the total length. The first image, captured during the initial surfacing phase, covered the rostrum to the anterior insertion of the dorsal fin (segments 1–10), from which we recorded the rostrum-to-dorsal-fin-insertion length and measured body width at each interval (Fig. 2A). The second image, taken as the animal transitioned into a dive, captured the region from the anterior insertion of the dorsal fin to the fluke notch (segments 11–22), from which we obtained the dorsal-fin-insertion-to-fluke-notch length and measured body width at each interval (Fig. 2B). Total length was calculated by summing the rostrum-to-dorsal-fin-insertion and dorsal-fin-insertion-to-fluke-notch lengths. Width measurements from both body sections were used to estimate body volume in subsequent modeling steps. This 2-part measurement approach was designed to capture a more accurate and consistent representation of length and volume when the whale was relatively flat and perpendicular to the imaging plane. All measurements were completed in MorphoMetriX (v.2) (Torres & Bierlich 2020).

2.2.2. Body volume estimation

Body volume calculations were adapted from Christiansen et al. (2019) and based on measurements from the 2-image approach, in which the false killer whale body was segmented into 22 discrete segments (S) along the longitudinal axis, defined by 21 evenly spaced width points (W). Each segment was modeled as a 3-dimensional (3D) solid of revolution, with the cross-sectional shape defined by width and height measurements at the segment boundaries and calculated using either an elliptical or tapered-area formula, depending on the anatomical tapering in that region. Height was estimated using height-to-width ratios (Christiansen et al. 2019) derived from measured adult (male and female) and non-adult (male and female) individuals in human care (n = 4). Male and female ratios were averaged within each age class, and the resulting mean adult ratio was applied to free-ranging adults, whereas the mean non-adult ratio was applied to calves and subadults according

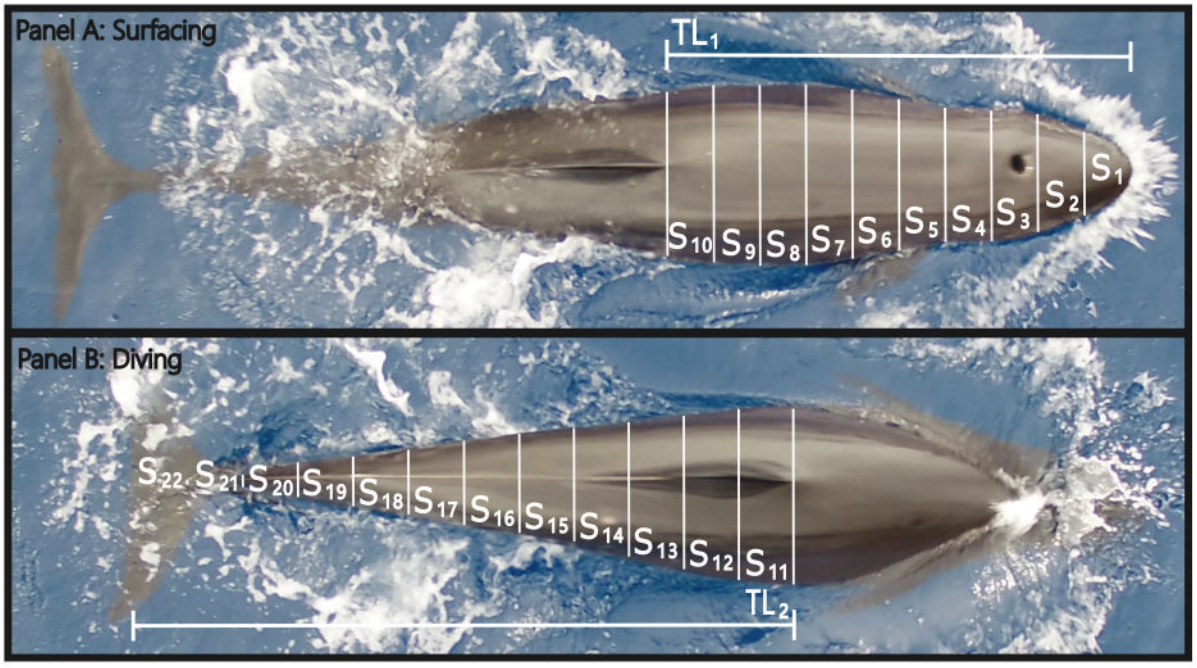

Fig. 2. Measurement of false killer whale body width and length: (A) surfacing image shows the length from the rostrum to the dorsal insertion, along with 10 width segments (S) across the body; (B) diving image shows the length from the dorsal insertion to the fluke notch, with 12 width segments recorded along the body

to assigned age class. Individuals in human care provided the most precise measurements because direct, controlled morphometric assessment minimized posture, perspective, and scaling error relative to field-based photogrammetry. Given that age-class-specific ratios were applied and derived from both adult and non-adult individuals, potential bias is expected to be minimal; however, unmeasured population-level differences (i.e. Hawai'i versus Japan) in height-to-width relationships could introduce minor scaling differences among age classes. To fully capture body shape variation (Baieri et al. preprint doi:10.48550/arXiv.2504.15782), the body volume of each false killer whale was calculated by dividing the body into 22 defined segments (S), with the methodology varying depending on the shape of the cross-section at each segment to obtain a more accurate representation of body volume (Fig. 3). Specifically, segments along the body were categorized into 2 broad shapes based on anatomical tapering: elliptical cross-sections and tapered cross-sections. Elliptical segments captured smoothly curved regions of the body, while tapered segments represented areas where the body narrows sharply in the dorso-ventral plane.

Segments categorized as elliptical (from 10–50% of the body length) were modeled using the area formula for an ellipse, where width and height at each segment boundary define the major and minor axes:

$$A(x) = \pi \times \left(\frac{w}{2}\right) \times \left(\frac{h}{2}\right) \quad (2)$$

where $A(x)$ is the cross-sectional area (m^2) at position x along the body and w and h are the width (m) and height (m) at the segment boundary. Tapered segments (from 0–10% and 50–100% of the body length) were modeled using a modified geometric function to approximate the sharp dorso-ventral narrowing:

$$A(x) = \frac{w \times h}{2} \quad (3)$$

The segment volumes were then computed by integrating the cross-sectional areas across the length of each segment, using the following integral:

$$v = \int_0^1 A(x)\mathrm{d}x \times L_{\text{total}} \times S_{\text{fraction}} \quad (4)$$

where L_{total} is the total body length and S_{fraction} represents the fraction of the total length occupied by each segment. Total body volume was obtained by summing the volume of all segments. This methodology was applied uniformly across all individuals and implemented in R (R Core Team 2025).

Calculated body volumes excluded the pectoral fins, dorsal fin, and fluke blades. Volume loss from nutritional stress is concentrated between the head and anus (Koopman et al. 2002), while appendages contain

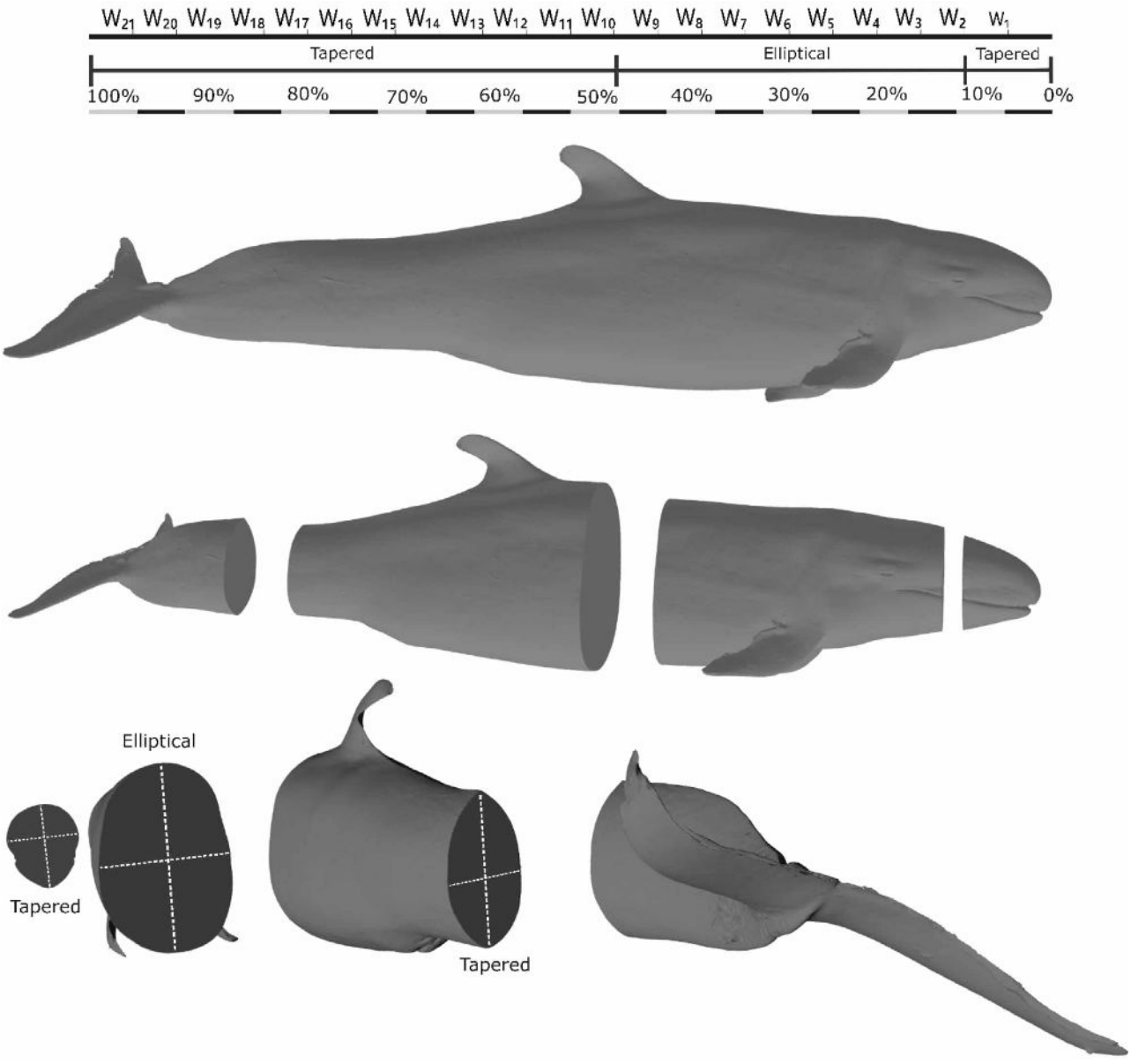

Fig. 3. Three-dimensional model of a false killer whale divided into 22 segments (S) to illustrate the volume estimation approach. Each segment volume was calculated by integrating the cross-sectional area along its length using width measurements (W) at segment boundaries, with total body volume derived from the sum of all segment volumes. See Text S1 for details on scanned image

minimal blubber and low lipid contents (Strandberg et al. 2008) and are therefore unlikely to significantly affect volume-based assessments of body condition if removed. Comparisons of 3D-scanned models of 6 false killer whales (see below) with appendages digitally removed in Meshmixer (Autodesk Research 2017) showed they contributed only 1.1–3.7% of total body volume (mean ± SD: 2.6 ± 1.1%).

To evaluate the accuracy of drone-based volume estimation methods, 9 false killer whales under human care at the Okinawa Churaumi Aquarium (Okinawa, Japan), the same drone, altimeter system, and elevation were used to compare composite images (combining surfacing and diving frames) and flat images (taken when the animal was lying flat at the surface) with 3D scan-derived body volumes. It is important to note that population-level morphological differences have been reported for false killer whales, primarily in overall body size, growth, and cranial characteristics (Ferreira 2008, Ferreira et al. 2014). Drone-based length and width measurements capture expected variation in body size, and any Japan-specific differ-

ences in body cross-sectional shape are unlikely to introduce substantial error into the volume approximations applied to free-swimming animals in Hawai'i. Animals were trained to remain still out of the water to allow for 3D-scanning using a handheld scanner (Leo, Artec3D), which provides a volume precision of 0.03% over 100 cm. White zinc marks were applied to the body because zinc is tolerated by the skin and provided necessary reference points in the absence of sufficient natural features, which ensured accurate merging of scans into a single full-body reconstruction. To reconstruct a 3D-image of the whole animal, scans were processed and merged in Artec Studio 14 Professional using 3–5 anatomical landmarks (e.g. blowhole, eyes, fin bases, fluke notch, or scars) and zinc marks when necessary. Missing data (i.e. gaps) were filled to create a watertight object for volumetric calculation. Final mesh adjustments were made in Meshmixer (Autodesk Research 2017) to ensure anatomical accuracy across merged sections. Only scans with complete coverage and minimal movement were used for volume estimation. Percent differences between drone-based body volumes and 3D scan-derived body volumes were calculated for each individual, and the mean ± SD of these differences was then computed across all individuals. The mean ± SD of these differences was used to quantify volume measurement uncertainty, which was then propagated through all subsequent volume-dependent measurements and analyses. These metrics were used to assess how closely each model approximated 3D scan-derived body volumes, determine which one was considered the most representative of the animal, and evaluate the reliability of each method for estimating false killer whale morphology.

2.2.3. Estimating body mass

To estimate the mass of free-ranging false killer whales, we combined body volume derived from photogrammetry with empirical estimates of tissue density from animals under human care, following methods used in previous cetacean studies (Christiansen et al. 2019, 2023, Glarou et al. 2023, van Aswegen et al. 2025c). Mean (±SD) body tissue density (ρ; kg m^{-3}) was calculated for 6 false killer whales under human care, ranging from 2 to 51 yr of age and weighing 326–630 kg, using known values of body mass (BM, measured with a scale) and 3D-scanned body volume (BV) as follows:

$$\rho = \frac{BM}{BV} \quad (5)$$

To incorporate uncertainty in body tissue density, body density was assumed to follow a normal distribution, and 1000 bootstrapped data sets were generated by random sampling with replacement. Individual body mass (BM_i) was then estimated as:

$$BM_i = BV_i \times \rho_i \quad (6)$$

where ρ_i is a randomly sampled tissue density value for individual i and accounts for natural variability in body composition. Given that body density was calculated from measured whole-body mass and 3D-derived whole-body volume, it inherently reflects the composite density of all tissues present at the time of measurement, including lean tissue, lipid stores, bone, viscera, and connective tissue. While this approach does not partition lipid and lean tissue explicitly, bootstrapping the observed density distribution allows natural variability in body composition to be incorporated into individual mass estimates.

2.2.4. Quantifying false killer whale body condition

To examine the relationship between body length and volume in false killer whales, we applied a log–log linear regression of the form:

$$\log(BV_i) = \alpha + \beta \times \log(BL_i) \quad (7)$$

where BV_i is the body volume of individual i (m^3), BL_i is the body length of individual i (m), and α and β are the intercept and slope, respectively. Ordinary least squares regression was used to estimate model parameters. Residuals were examined to assess model fit and adherence to standard linear regression assumptions.

To quantify variation in body condition among social clusters, we generated 1000 bootstrapped data sets by resampling individual body length and volume with replacement, incorporating established measurement errors. Measurement uncertainty was quantified as the mean ± SD of the percent difference between drone-based estimates and reference measurements derived from 3D scans for body volume (m^3) and direct physical measurements for length (m).

Each bootstrapped data set was used to fit a regression model, producing distributions of slope and intercept values. The mean slope and intercept were then used to calculate expected body volume, BV_{exp}, for each individual based on its total length:

$$BV_{exp} = \beta_0 + \beta_1 \times BL_i \quad (8)$$

where β_0 and β_1 represent the bootstrapped intercept and slope, respectively. Individual body condition was expressed using a BCI, defined as the residual between observed and expected volume:

$$BCI_i = \frac{BV_{obs,i} - BV_{exp,i}}{BV_{exp,i}} \quad (9)$$

BCI_i represents the BCI for false killer whale i, $BV_{obs,i}$ is the observed body volume, and $BV_{exp,i}$ is the expected body volume given their length, for the same individual.

2.3. Data analysis

2.3.1. Changes in relative body width with age class

To examine age-class differences in body shape and blubber storage, we measured relative body width (% body length) at each segment (~4.5%) for the entire body length for each individual using the surfacing and diving images. Body width measurements were normalized as a percentage of total body length to obtain relative body width (Christiansen et al. 2024). We then grouped the data by age class (calf, subadult, adult) as recorded in the field or at the time of UAS review based on the length of the individual when the measurement was taken, following morphological criteria adapted from Bearzi et al. (1997). Specifically, adults were assigned based on observer experience considering body size, morphology, and behavior; calves were defined as individuals approximately half the length of the associated adult; and subadults were approximately three-quarters the length of an adult. Newborns, typically characterized by fetal crease marks and in close and constant association with an adult (Bearzi et al. 1997), were not present in this data set. Calves included in the analysis were likely at least 1 yr old, based on their size and the absence of fetal folds, which disappear within weeks to several months after birth (Mann et al. 2000a). The mean (±SD) relative body width were calculated for each site within each age class.

2.3.2. Body volume and length relationships across social clusters

To evaluate differences in body condition among social clusters, we applied standardized major axis (SMA) regression (Warton et al. 2006) to examine the allometric relationship between log-transformed total body length and body volume, using the 'smatr' package in R (Warton et al. 2012). SMA was selected because both variables contain measurement errors and follow a biological power-law scaling relationship. To account for uncertainty, we generated 1000 bootstrapped data sets by resampling individual length and volume values with normally distributed noise, where the distribution parameters were derived from the mean ± SD of percent differences between drone-derived estimates and validation measurements obtained from 3D scans (volume) and direct physical measurements (length). Given that SMA estimates structural scaling relationships rather than individual trajectories, and because inference was based on bootstrapped resampling, repeated measures of individuals do not violate SMA assumptions.

Each bootstrapped data set was analyzed independently using SMA regression. For each iteration, we first tested whether social clusters shared a common slope. Iterations with a p-value of > 0.05 were interpreted as supporting a common slope, permitting subsequent comparison of elevation (i.e. intercept). In these cases, elevation tests were used to assess whether social clusters differed in body volume at a given length, providing insight into potential differences in body condition.

2.3.3. Evaluating BCI

To assess differences in BCI among social clusters, analyses were restricted to adult individuals from the 3 social clusters encountered (Clusters 1, 2, and 4) to minimize variation associated with ontogenetic growth. Excluding calves and subadults reduced confounding effects from differing metabolic demands, growth patterns, and body proportions (Balčiauskas & Balčiauskienė 2024b). Potential effects of sex were not evaluated because sex was available for only 17.8% of measured individuals, providing an insufficient sample size for analysis. BCI values reflect individual deviations from expected body volume given length, where negative values indicate leaner-than-expected condition, zero represents average condition, and positive values reflect above-average condition (Christiansen et al. 2016, 2018). Julian day, year, and season were included as covariates to account for seasonal and interannual variation in body condition. Season was categorized into 4 levels based on sea surface temperature (Flament 1996) and to align with other studies on false killer whales (Baird et al. 2021): winter (February–April), spring (May–July), summer (August–October), and fall (November–January). A linear mixed-effects ANOVA was conducted to test for differences in BCI with individual identification

included as a random intercept to account for repeated measurements of the same individual. Model assumptions, including normality (Shapiro-Wilk), homogeneity of variance (Levene's test; car package; Fox 2019), and linearity (residual diagnostics), were assessed.

To identify biologically meaningful changes in body condition, we defined thresholds as an absolute BCI change of ≥0.1 and at least 1.5 times the individual's SD. All individuals with at least one resight (i.e. 2 or more sightings) were assessed. This dual threshold ensured both ecological relevance and statistical robustness. The 0.1 criterion reflects meaningful shifts in fat and muscle mass, particularly when BCI is calculated as the residual from a body volume–length regression (Cattet et al. 2002, Shirane et al. 2020, Balčiauskas & Balčiauskienė 2024a).

3. RESULTS

From 2019 to 2025, a total of 142 photogrammetric measurements, including resights, were obtained, consisting of 118 adults, 16 subadults, and 8 calves, with 3 individuals transitioning from calf to subadult during this period. These included 57 measurements from Cluster 1 (17 individuals), 16 from Cluster 2 (14 individuals), 66 from Cluster 4 (33 individuals), and 4 from unidentified individuals (Table S1 in the Supplement at www.int-res.com/articles/suppl/esr01505_supp.pdf). These measurements represented 64 distinct false killer whales, plus 4 individuals with indistinct dorsal fins, from 3 of the 4 social clusters of the endangered MHI insular population. Across all individuals included in the analyses, total body length averaged (±SD) 3.99 ± 0.65 m and ranged from 2.16 to 5.28 m. Given that the unidentified individuals were consistently seen with known members of Clusters 1, 2, or 4 and in locations typical of those clusters, it is likely that they belonged to one of these groups, making Cluster 3 membership unlikely.

3.1. Changes in relative body width with age

Relative body width declined with age class (Fig. 4), with calves exhibiting the highest mean relative widths at 15.8% of total body length. This pattern was most pronounced in the 25–45% body length region, where fat reserves are typically stored. Subadults followed a similar distribution but with lower peak values (13.7%), and adults showed the narrowest profiles overall.

3.2. Body volume estimation

Based on the 9 animals in human care, the average (±SD) composite volume estimates differed from 3D-scanned volumes by 2.12 ± 2.53%, while flat volume

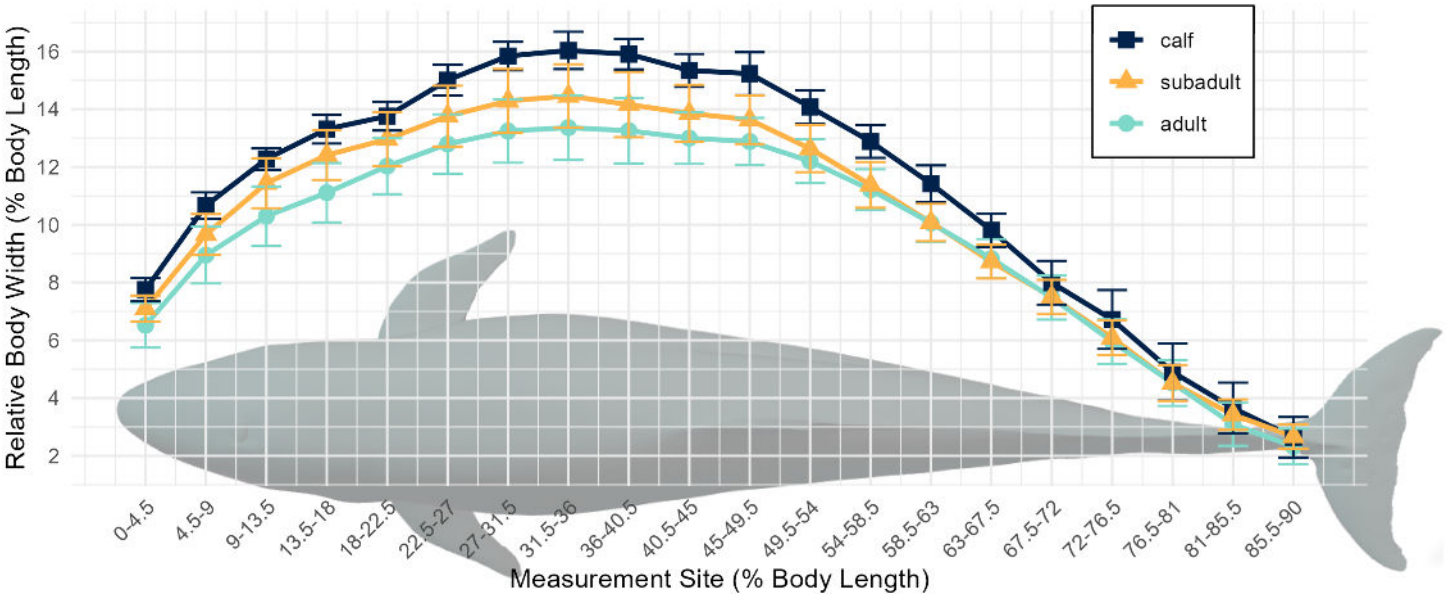

Fig. 4. Relative body width (% body length) measured at different body-length sites across age classes of false killer whales. The plot displays the mean (±SD) relative body width at each measurement site for calves, subadults, and adults

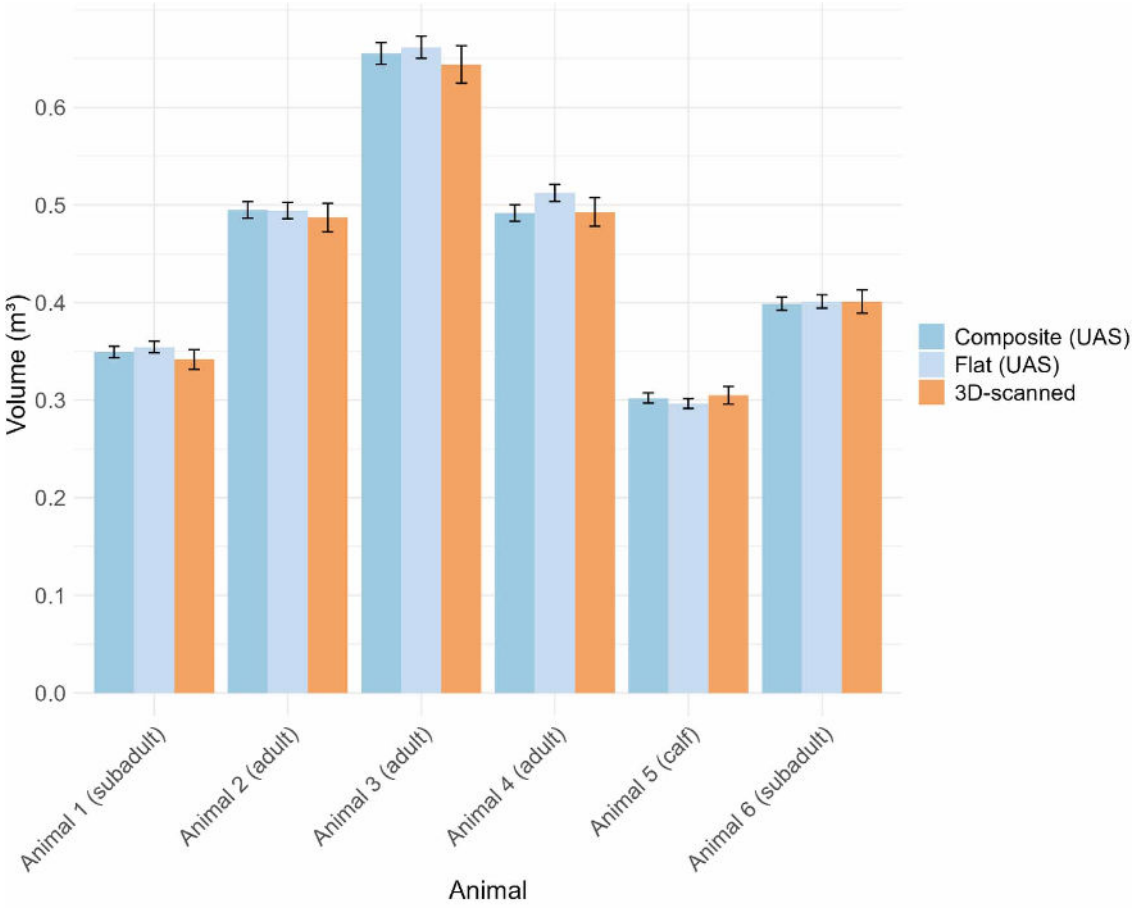

Fig. 5. Volume measurements of 6 false killer whales in human care, as determined from drone-based measurements using 2 techniques (i.e. composite and flat) and 3D scans. Error bars represent measurement uncertainties, with 3% error for the 3D scan based on manufacturer specifications and 1.7% error for drone (UAS) measurements based on Vivier et al. (2023)

estimates showed a slightly higher average difference of 2.73 ± 1.91% (Fig. 5). These results indicate that the composite method more closely approximated 3D-scanned body volume and provides a reliable basis for estimating body condition in false killer whales. Comparison of drone-based photogrammetric estimates with reference measurements obtained from 3D-scans for body volume and direct physical measurements for body length yielded a measurement uncertainty of 3.76 cm (0.7–1.8%) for length and 0.0060 m^3 (0.9–1.7%) for volume. These values represent the SD of the differences between drone-derived and reference measurements and were used as measurement error in subsequent analysis.

3.3. Body volume and length relationships across social clusters

SMA regressions of log-transformed body length and volume revealed strong, significant relationships within each social cluster (Cluster 1: $R^2 = 0.904$, $p < 0.001$; Cluster 2: $R^2 = 0.927$, $p < 0.001$; Cluster 4: $R^2 = 0.937$, $p < 0.001$; Fig. 6). Across 1000 bootstrapped iterations, slopes differed significantly among social clusters, with the common slope hypothesis rejected in all iterations (100%). The p-values from the common slope tests were consistently significant (median $p < 0.001$), indicating distinct allometric scaling relationships between body length and volume. As slope heterogeneity violates the assumption of equal scaling, intercept comparisons were not performed.

3.4. Assessing false killer whale length, volume, and body condition

Across all individuals, body volume scaled positively with body length on a log–log scale, consistent with a power law relationship (volume $\propto$ length$^{2.44}$; 95% CI: 2.33–2.55; Fig. 7A).

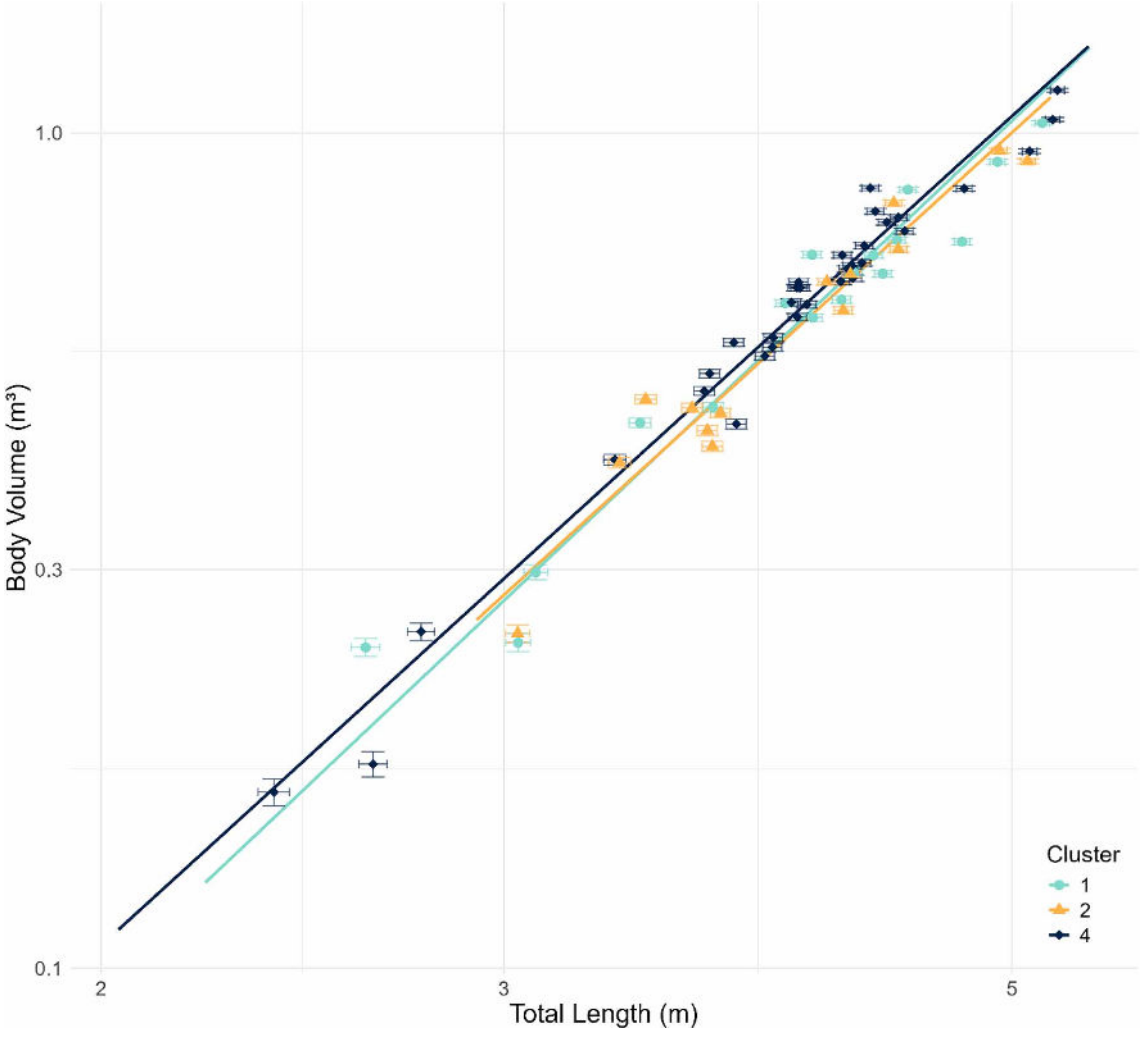

Fig. 6. Standardized major axis (SMA) regression of total body length versus body volume for false killer whale social clusters. Each line represents the SMA regression for a specific social cluster; points indicate mean total length and mean body volume for bootstrapped individuals within each social cluster, with associated 95% CI

Social clusters 1 and 4 exhibited similar scaling exponents in the length–volume relationship, suggesting consistent body condition scaling across body sizes. Cluster 4 had the best fit (R^2 = 0.96), indicating low variation in body shape. By contrast, Cluster 2 displayed a shallower slope and higher intercept, suggesting that smaller individuals in this cluster may have relatively greater volume, but gain volume more slowly as length increases. However, these patterns should be interpreted with caution due to wider CIs and a small sample size (n = 15 individuals from Cluster 2), and because this cluster had the fewest sightings, the absence of smaller or younger individuals is likely a sampling artifact rather than a true difference in size structure.

3.5. Evaluating BCI

Model selection for the linear mixed-effects ANOVA was based on sequential *F*-tests and AIC comparisons. The initial model included social cluster, year, Julian day, season, and a cluster × year interaction. The interaction term was not significant (p = 0.580), and its removal did not reduce model fit. Julian day (p = 0.660) and season (p = 0.121) also had no significant effect and were excluded from the final model, which retained only social cluster number and year as fixed effects. BCI differed marginally by year ($F_{2,109}$ = 2.31, p = 0.051) and significantly by cluster number ($F_{5,109}$ = 3.76, p = 0.040), indicating variation in body condition (Fig. 8, Table 1; Fig. S1, Table S2). Cluster 4 had the highest mean BCI across

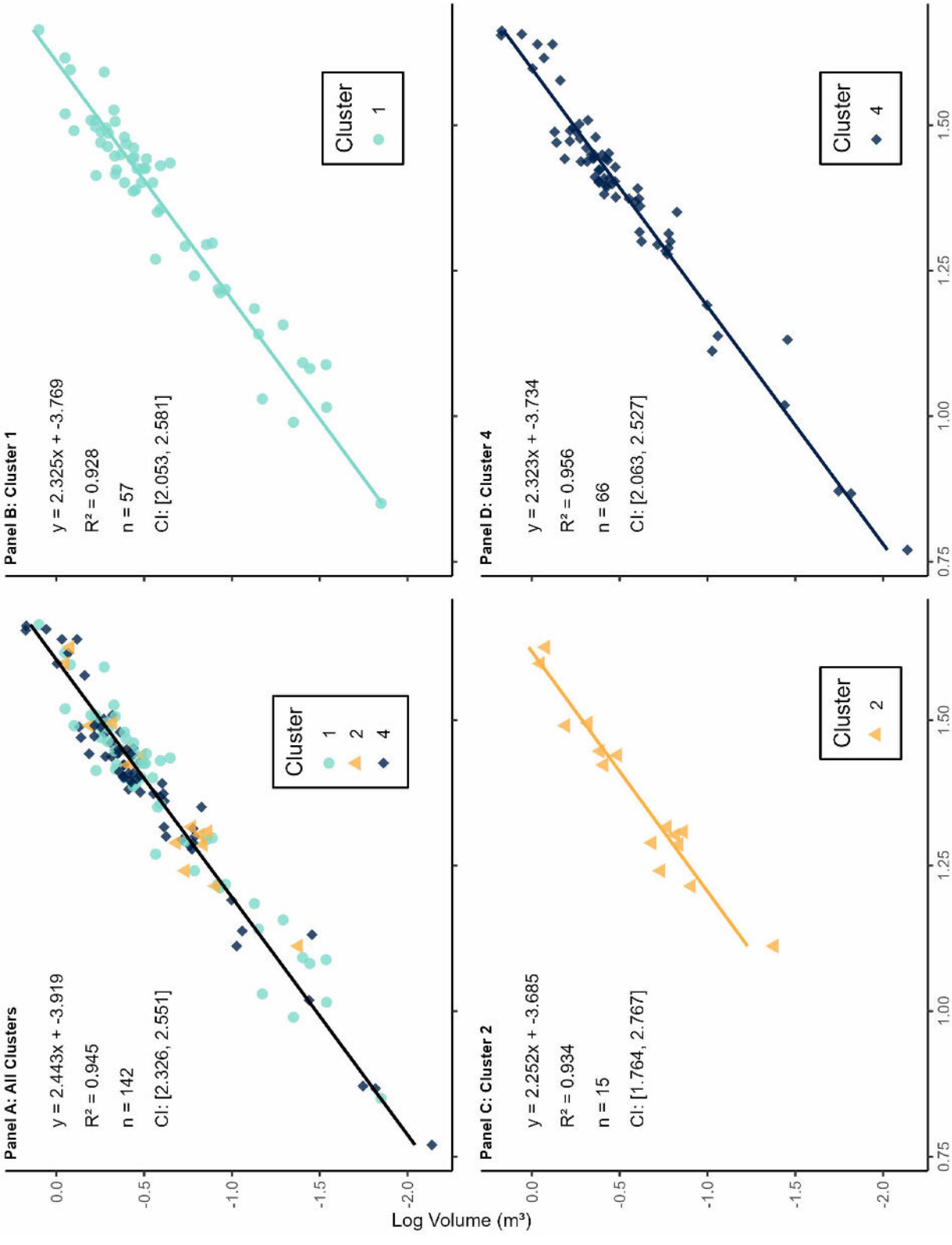

Fig. 7. Plots of log–log regression of body volume vs. body length for false killer whales, showing data (A) combined across all individuals and (B–D) cluster-specific regressions for Clusters 1, 2, and 4, respectively, illustrating differences in scaling relationships among social clusters

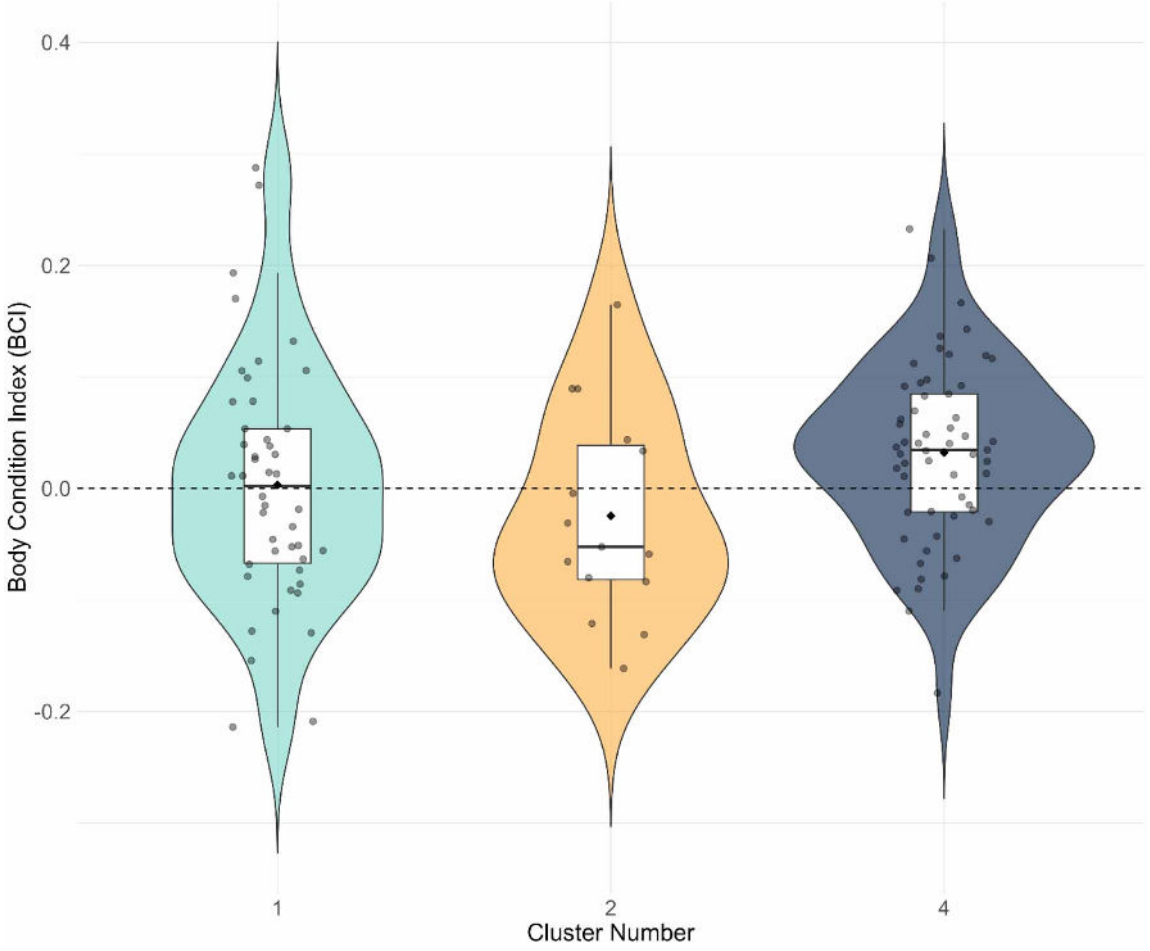

Fig. 8. Distribution of body condition index across false killer whale social clusters from 2019–2025. Boxplot inserts show the interquartile range, median values, and mean (black diamond)

years, followed by Clusters 1 and 2 (Fig. 8). The lowest average BCI occurred in 2020 (−0.025 ± 0.066), suggesting reduced body condition across all social clusters during that year (Fig. 9).

All model assumptions were met: BCI values were normally distributed within social clusters (Shapiro-Wilk, $p > 0.05$), variances were homogeneous (Levene's test, $p > 0.05$), residuals met normality (Shapiro-Wilk, $p > 0.05$), and no heteroscedasticity was detected (Breusch-Pagan test, $p > 0.05$).

3.6. Individual fluctuation in BCI

Three adult false killer whales from Cluster 1 met the thresholds for biologically meaningful change in BCI over time (Pacific Whale Foundation [PWF] #0078/Cascadia Research Collective [CRC] HIPc0272, PWF #0086/CRC HIPc0363, and PWF #0109/CRC HIPc0320) (Fig. 10). This contrasts with the remaining individuals, which exhibited relatively stable BCI values across resight intervals, with fluctuations remaining below the predefined threshold for biologically meaningful change (Fig. S2). The sex of these individuals was unknown, but varied in both size and maximum estimated body mass, with time differences between measurements shown in Fig. 10:

- #0078 measured 4.5 m with a mass of 1006 kg (95% CI: 993.5–1018.5 kg; measurement range: 999.8–1012.2 kg);
- #0086 measured 3.6 m with a mass of 574 kg

Table 1. Linear mixed-effects ANOVA results showing the effects of social cluster number and year on false killer whale body condition index

Variable	SS	MS	df	*F*	p
Cluster number	0.039	0.019	2	3.375	0.040
Year	0.066	0.013	5	2.305	0.051

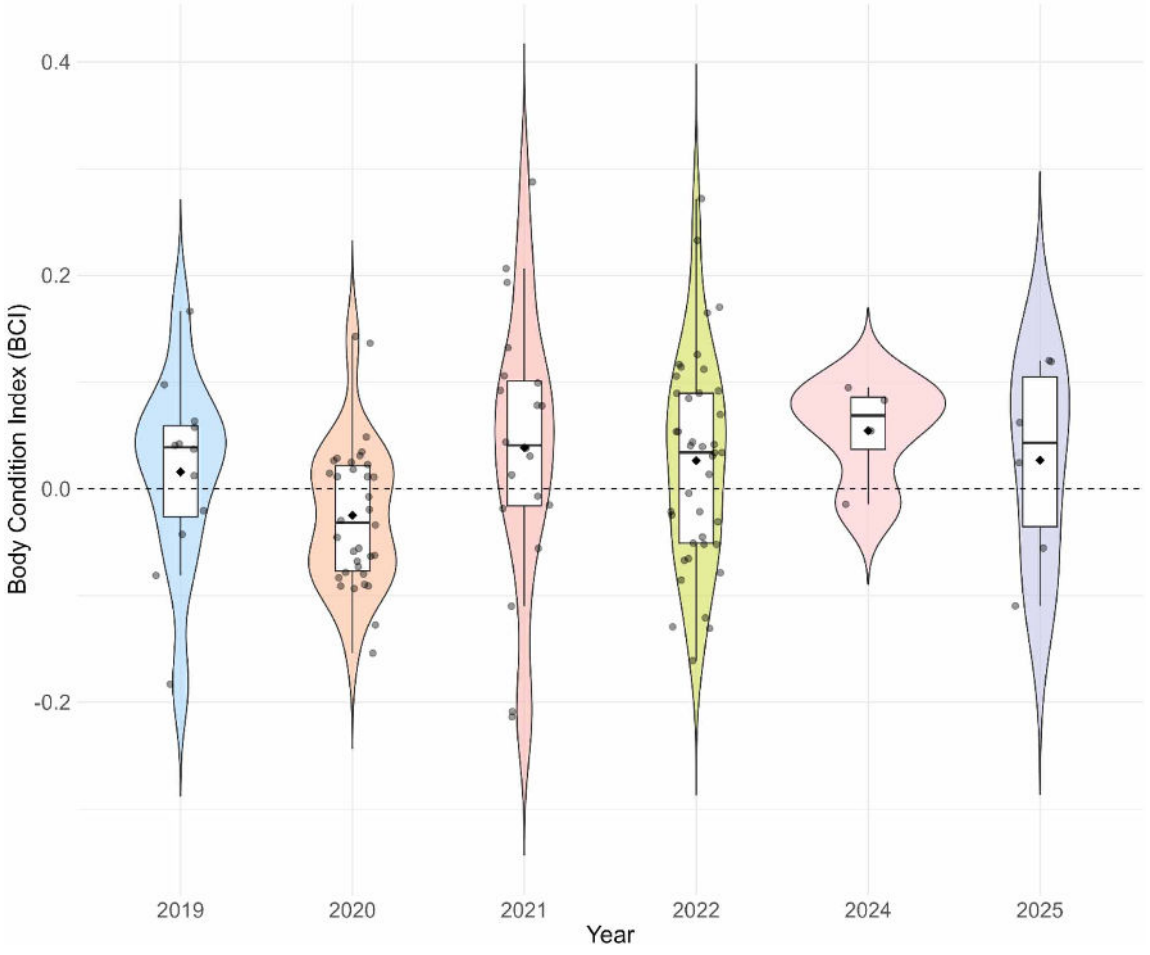

Fig. 9. Distribution of false killer whale body condition index across years for all individuals, regardless of cluster membership. Boxplot inserts show the interquartile range, median values, and mean (black diamond). Data from 2023 were excluded due to an insufficient number of sightings

(95% CI: 561.5–586.5 kg; measurement range: 567.8–580.2 kg);

- #0109 measured 4.2 m with a mass of 832 kg (95% CI: 819.5–844.5 kg; measurement range: 825.8–838.2 kg).

Body mass estimates were derived from volume measurements using a mean (±SD) tissue density of 1052.9 ± 55.8 kg m^{-3}, representing the composite density of all body tissues, including lean tissue, lipid stores, bone, and viscera. Estimated mass loss between sightings ranged from 146 kg (#0086) to 234 kg (#0109), representing declines of 25–28% of body mass. Across all 3 individuals, a decrease in BCI of 0.1 corresponded to an average mass loss of 104.4 ± 42.2 kg, representing a mean reduction of 14.4 ± 4.7% in body mass. With the exception of individual #0078, which in 2021 was observed on one occasion with a calf swimming in close proximity, all sightings of these individuals occurred either as lone animals or, in a few cases, within small groups of 3–5 conspecifics. No atypical behaviors were observed during measurement encounters, and individuals appeared to be swimming and traveling normally. Individual #0109 showed recovery to a positive BCI following multiple fluctuations. By contrast, #0086 remained close to neutral or negative condition across all sightings and exhibited visible signs of poor health, including a sunken blowhole (Fig. S3).

4. DISCUSSION

This study first validated UAS-derived photogrammetry for false killer whales by ground-truthing composite volume estimates against 3D-scanned volume measurements from individuals under human care, providing methodological confidence in the approach. We then applied this technique to the MHI insular

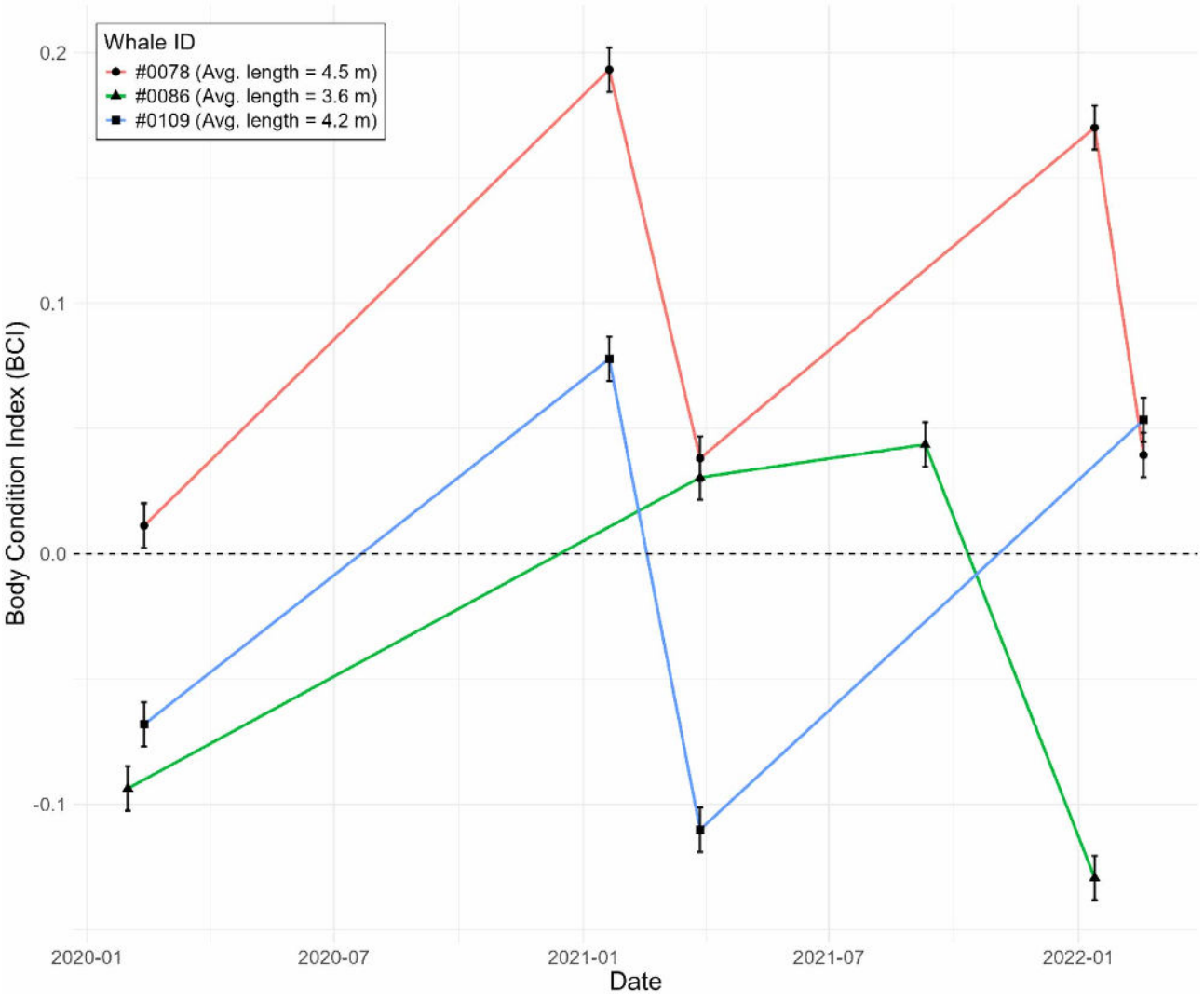

Fig. 10. Temporal variation in estimated body condition index (BCI) for repeatedly measured false killer whales from Cluster 1. Each line represents an individual that experienced an absolute change of ≥0.1 in BCI that was also 1.5 times the SD. Vertical error bars represent a fixed uncertainty in volume estimates. Sex was unknown for all 3 individuals

population to generate the first body condition estimates for this endangered population, comparing BCI across 3 of the 4 social clusters and evaluating individual-level fluctuations over time. Body volume scaled differently with length across social clusters, with Clusters 1 and 4 exhibiting, on average, higher body condition. The data set spans 64 known individuals (4 unknown) across age classes, representing approximately half the current population size, and offers a valuable baseline for future health monitoring at both the individual and population levels.

The observed decline in relative body width with age class is consistent with a shift from early-life lipid store accumulation to increased energetic demands in adulthood, as reported in humpback whales *Megaptera novaeangliae* (van Aswegen et al. 2025a). Younger false killer whales exhibited the highest relative fat energy reserves (inferred from width measurements), reflecting a critical period for energy storage and likely indicating substantial maternal investment during the early years of independence (van Aswegen et al. 2025a). Studies of blubber structure reinforce this interpretation, where blubber is a stratified tissue with distinct layers serving different functions, with the middle layer acting as a lipid reservoir and the inner layer more metabolically dynamic and responsive to energetic demands (Gómez-Campos et al. 2015, Phipps et al. 2023). In false killer whales, adipocyte area and index (i.e. the size of lipid-filled fat cells) varied across layers and body regions, with anterior—ventral regions showing the greatest lipid storage potential (Phipps et al. 2023), similar to other odontocetes,

where ventral blubber was identified as a primary site for energy storage and mobilization (Gómez-Campos et al. 2015). This pattern of early-life lipid storage, resulting from significant maternal investment, is well documented in baleen whales (Christiansen et al. 2023, van Aswegen et al. 2025c) and other marine mammals (Mann et al. 2000b). Short-finned pilot whales *Globicephala macrorhynchus* exhibited similar trends, with calves having the highest relative body width among age classes (Arranz et al. 2022). The elevated energy stores in calves may reflect the outcome of prolonged maternal provisioning. However, additional factors such as foraging ecology (Hersh et al. 2025) and population-specific thermoregulatory demands (Favilla et al. 2024) may contribute to differences among species and populations, warranting further investigation. These findings underscore the importance of early-life energy storage and highlight the potential vulnerability of calves to fluctuations in prey availability. Specifically, reductions in maternal foraging success could compromise calf survival while also affecting maternal condition. Further research is needed to examine how variability in fat reserves and provisioning influences fitness in the context of continued population decline (Badger et al. 2025).

The close agreement between drone-based and 3D-scanned volume measurements (<3% difference) demonstrates the precision of UAS photogrammetry for tracking fine-scale changes in body volume (Currie et al. 2021) and estimating body mass (Christiansen et al. 2019, van Aswegen et al. 2025b). However, interspecific differences in body shape require caution when converting volume to mass, where accurate shape characterization is essential (Christiansen et al. 2019). Morphological differences among false killer whale populations have been documented, including variation in total length, growth parameters, and cranial morphology (Ferreira 2008, Ferreira et al. 2014). Differences in body cross-sectional geometry, which is the basis for our volume calculations, are unknown, and the use of whales from Japan to derive volume estimates may therefore introduce some bias, which is noted as a potential limitation. However, this approach is markedly more accurate than applying a generalized ellipsoid model, which would have overestimated false killer whale volume by 10–15%. These findings underscore the value of species-specific shape modeling and highlight the important role of animals under human care in validating remotely collected morphometric data and to support conservation of free-ranging populations (Kuczaj 2010).

Variation in how body volume scales with length across social clusters suggests that nutritional stress may vary among social clusters, potentially reflecting differences in foraging strategies, efficiency, and prey availability. However, uneven sample sizes across social clusters may have contributed to the observed differences in scaling and should be considered when interpreting these results. False killer whale social clusters occupy numerous distinct and persistent high-use areas (Baird et al. 2012, Mahaffy et al. 2023), maintain long-term social bonds, and exhibit social cluster-specific spatial and dietary niches that vary in their degree of overlap, with some clusters showing substantial spatial and isotopic overlap (e.g. Clusters 1 and 3) and others being more distinct (e.g. Clusters 2 and 4) (Baird et al. 2012, 2023, Kratofil et al. preprint doi:10.64898/2026.02.06.704493). These ecological and behavioral differences suggest that variations in spatial ecology could contribute to differences in body condition among social clusters.

Clusters 1 and 4, which showed similar body length–volume scaling relationships, both use multiple high-use areas and share a high-use area north of Molokaʻi, and Cluster 1 also shares a high-use area with Cluster 2 off Hawaiʻi Island and within the ʻAlenuihāhā Channel (Baird et al. 2023). By contrast, Cluster 2 exhibited a significantly shallower slope, consistent with reduced body condition, and occupies a more concentrated high-use area off Hawaiʻi Island and northeast Maui. However, this pattern should be interpreted with caution because the comparatively small sample size and limited size range of Cluster 2, likely resulting from low sighting rates and the underrepresentation of smaller or younger individuals, may have influenced the observed relationship. Notably, the shared areas used by Clusters 1 and 4 north of Molokaʻi and Cluster 2's high-use area have the highest fishery overlap indices, which combine metrics on the number of licenses, fishing days, and total catch with false killer whale distribution (Baird et al. 2021). Evidence of fisheries interaction is present in 20–25% of individuals across all 3 social clusters and was observed in ~33% of the measured individuals, highlighting the widespread and persistent nature of this competition (Baird et al. 2015, Harnish et al. 2024). The extent to which fisheries interactions directly influence body condition remains unresolved and represents an important topic for future research.

Differences in body condition among social clusters are unlikely to be driven by contaminant-related physiological effects, with no clear association between contaminant load and body condition (Kratofil et al. 2020). Cluster-level differences in some persistent organic pollutants, including summed concentrations of polybrominated diphenyl ethers (ΣPBDEs), after

accounting for known factors such as reproductive status, are likely attributable to differences in foraging habitat that vary in pollutant exposure (Kratofil et al. 2020). Although contaminant burden is unlikely to be a primary driver of body condition differences, reduced body condition can exacerbate the physiological effects of lipophilic contaminants through mobilization of endogenous lipid stores, particularly during periods of nutritional stress (Lundin et al. 2016, Wasser et al. 2017). However, more data across a broader size range for Cluster 2 would help confirm these patterns and clarify drivers of body condition differences among social clusters.

Individual trajectories underscore substantial variation in nutritional status and recovery potential, with 3 adults from Cluster 1 exhibiting marked fluctuations in BCI across years. Pregnancy status could not be assessed for any individual during the study period. Although undetected pregnancy cannot be ruled out, the absence of observed calves during most encounters and the lack of atypical behavior suggest that measured individuals were not experiencing obvious reproductive or behavioral states that might systematically bias the observed patterns. Clusters 1 and 3 exhibit the widest spatial use among social clusters (Baird et al. 2023), possibly reflecting reduced foraging efficiency and a greater need to travel in search of prey. However, core areas reflect multiyear averages across multiple individuals, whereas body condition is shaped by individual movement that can vary substantially both within and among clusters (M. A. Kratofil pers. comm.). The larger core area used by Cluster 1 may contribute to poorer body condition through increased travel costs, but local prey quality and density, together with fine-scale individual movement, are also likely to influence foraging success and nutritional state. Increased movements likely increase energetic costs (Allen et al. 2022, Williams & Davis 2024), which may be consistent with the volume changes documented here and with patterns reported in other cetaceans under foraging stress (Foster et al. 2012, Currie et al. 2021). Future work integrating individual-level telemetry with repeated photogrammetric assessments of BCI would help clarify links between short-term space use and nutritional state at the individual level. Despite their high metabolic demands, odontocetes of similar size can tolerate substantial reductions in body mass (Currie et al. 2021). Foraging cessation may result in daily losses of approximately 2% of body mass, with the capacity to withstand up to 27% total mass loss (Currie et al. 2021). However, mortality risk is likely very high at such extremes, with survival outcomes uncertain, as evidenced by pygmy killer whales *Feresa attenuata* stranding and dying after losing 13–14% of their body mass within 1 wk (Currie et al. 2021), which corresponds to an average BCI change of 0.1 for false killer whales. For smaller odontocetes, these losses can reach 5% d^{-1} and several mm of blubber thickness (Kastelein et al. 2019). These findings suggest that spatial ecology and availability of quality prey may be key drivers of body condition. Understanding individual- and social cluster-level foraging strategies is therefore critical to evaluating population vulnerability, particularly in systems where energetic constraints may amplify the effects of prey depletion and competition.

Marginally significant interannual variation in BCI, particularly the decline observed in 2020, highlights substantial fluctuations in population health. These changes may be driven by annual shifts in prey availability, environmental variability, and human-induced stressors, all of which are known to influence cetacean body condition (Bradford et al. 2012, Durban et al. 2016, Christiansen et al. 2020, 2024, Kotik et al. 2023, Napoli et al. 2024, Serres et al. 2024). In particular, 2019 saw record sea surface temperatures in Hawaiian waters (NOAA Coral Reef Watch 2025) due to a major marine heatwave raising temperatures 2.5°C higher than normal throughout the North Pacific (Amaya et al. 2020), triggering a significant coral bleaching event in Hawai'i (Winston et al. 2022). Such heatwave and bleaching events are known to disrupt reef ecosystems and can lead to declines in reef-associated fish abundance and availability (Pratchett et al. 2011), leading to wider spread food web impacts (Pratchett et al. 2008). These environmental and ecological stressors may have contributed to the lower average BCI observed in 2020. This decline preceded a stranding event in February 2021, where a single individual from Cluster 4 stranded on the north shore of Maui (University of Hawai'i News 2021). However, it is important to note that strandings represent only a small and often random subset of mortality events, known to occur for this population each year, and in this case, no published information was available on the individual's health condition at death or the cause of stranding.

Our findings reinforce the value of long-term BCI monitoring to detect health trends and anticipate population-level consequences of ecological stress. The MHI insular population has declined steadily over the past decade (i.e. 2012–2022; Badger et al. 2025), and the poor condition observed in certain years or individuals may signal elevated mortality risk, as reported in other cetaceans (Christiansen et

al. 2020, 2021, Stewart et al. 2021a,b). Notably, 2020 had both the lowest average BCI and the largest single-year population decline (~10%) in the last 5 yr (Badger et al. 2025), mirroring patterns observed in killer whales *Orcinus orca* under nutritional stress (Durban et al. 2021). These variable body condition patterns may also reflect the costs of long-term residency in an oligotrophic environment, where limited and unpredictable prey resources can constrain energy intake for a top predator. Persistent site fidelity in such systems may increase vulnerability when environmental conditions shift, potentially functioning as a maladaptive strategy under rapid ecological change, as seen in other taxa (Merkle et al. 2022). These patterns are consistent with observations in other species, such as humpback whales, where marine heatwaves on high-latitude feeding grounds have been linked to reduced prey availability, declines in abundance (Frankel et al. 2022, Cheeseman et al. 2024), and lower reproductive rates (Cartwright et al. 2019). Continued monitoring of both abundance and condition will be essential for linking individual health to demographic trends and informing conservation efforts (Durban et al. 2021, Stewart et al. 2021a).

Our findings are consistent with emerging research linking metabolic demands and prey quality to body condition in odontocetes (Currie et al. 2021, Durban et al. 2021). In ecosystems where high-energy prey becomes less accessible due to environmental or anthropogenic pressures, individuals may shift to lower-quality prey, leading to energetic deficits and declining condition. Given the apparent reliance of false killer whales on large pelagic and reef-associated game fish (Baird et al. 2021), continued reductions in fish abundance and size in Hawaiian waters (Oleson et al. 2010) are likely to exacerbate nutritional stress. Integrating dietary analysis with energetic modeling will be critical to quantifying these pressures and informing conservation strategies.

This study provides the first quantitative assessment of body condition in the endangered MHI insular false killer whale population, revealing variation across social clusters and within individuals over time. Differences in body condition within and between social clusters suggest that a combination of spatial ecology and prey availability is likely to contribute to nutritional stress. Continued integration of photogrammetry with ecological and energetic data will be essential for guiding conservation strategies and assessing population resilience in the face of environmental and anthropogenic changes.

Acknowledgements. The authors thank Florence Sullivan, Abigail Machernis, and Shannon Barber-Meyer from Pacific Whale Foundation as well as Gussie Hollers and Bri Madrigal from the Marine Mammal Research Program at the University of Hawai'i Mānoa for help with field data collection. We thank Sabre Mahaffy for her critical contributions in developing the social cluster designations used in this study, as detailed in her 2023 paper. We also thank Joshua Madin for providing the 3D-scanner to scan the false killer whales in human care. The present work was part of J.C.'s PhD thesis. We thank members and supporters of the Pacific Whale Foundation for providing partial funding to conduct this study, with particular gratitude to Mike and Kim Beauvais for their sustained support of the Pacific Whale Foundation and to Mike for his dedication to false killer whale research and conservation. Field work and equipment were also partially funded by Federal Award No. ONR N00014-22-S-B001 and NA19NMF4720181. This paper represents HIMB and SOEST contribution numbers 2035 and 12079, respectively.

LITERATURE CITED

Allen AS, Read AJ, Shorter KA, Gabaldon J, Blawas AM, Rocho-Levine J, Fahlman A (2022) Dynamic body acceleration as a proxy to predict the cost of locomotion in bottlenose dolphins. J Exp Biol 225:jeb243121

Amaya DJ, Miller AJ, Xie SP, Kosaka Y (2020) Physical drivers of the summer 2019 North Pacific marine heatwave. Nat Commun 11:1903

Arranz P, Christiansen F, Glarou M, Gero S and others (2022) Body condition and allometry of free-ranging short-finned pilot whales in the North Atlantic. Sustainability (Basel) 14:14787

Autodesk Research (2017) Meshmixer. https://www.research.autodesk.com/projects/meshmixer/

Badger JJ, Baird RW, Johnson DS, Bradford AL and others (2025) Accounting for sampling bias reveals a decline in abundance of endangered false killer whales in the main Hawaiian Islands. Endang Species Res 57:325–340

Baird RW (2009) A review of false killer whales in Hawaiian waters: biology, status, and risk factors. Report prepared for the US Marine Mammal Commission by Cascadia Research Collective, Olympia, WA

Baird RW, Gorgone AM, McSweeney DJ, Webster DL and others (2008) False killer whales (*Pseudorca crassidens*) around the main Hawaiian Islands: long-term site fidelity, inter-island movements, and association patterns. Mar Mamm Sci 24:591–612

Baird RW, Hanson MB, Schorr GS, Webster DI and others (2012) Range and primary habitats of Hawaiian insular false killer whales: informing determination of critical habitat. Endang Species Res 18:47–61

Baird RW, Mahaffy SD, Gorgone AM, Cullins T and others (2015) False killer whales and fisheries interactions in Hawaiian waters: evidence for sex bias and variation among populations and social groups. Mar Mamm Sci 31:579–590

Baird RW, Anderson DB, Kratofil MA, Webster DL, Mahaffy SD (2019) Cooperative conservation and long-term management of false killer whales in Hawai'i: geospatial analyses of fisheries and satellite tag data to understand fishery interactions. https://wildlifecomputers.com/blog/cooperative-conservation-and-long-term-management-of-false-killer-whales-in-hawai%CA%BBi/

Baird RW, Anderson DB, Kratofil MA, Webster DL (2021) Bringing the right fishermen to the table: indices of overlap between endangered false killer whales and nearshore fisheries in Hawai'i. Biol Conserv 255:108975

Baird RW, Cornforth CJ, Mahaffy SD, Lerma JK, Harnish AE, Kratofil MA (2023) Field studies and analyses from 2020 through 2022 to support the cooperative conservation and long-term management of main Hawaiian Islands insular false killer whales. Cascadia Research Collective. https://cascadiaresearch.org/publications/baird_etal_2023_section6/

Balčiauskas L, Balčiauskienė L (2024a) Extreme body condition index values in small mammals. Life (Basel) 14:1028

Balčiauskas L, Balčiauskienė L (2024b) Insight into body condition variability in small mammals. Animals (Basel) 14:1686

Bearzi G, Notarbartolo-DI-Sciara G, Politi E (1997) Social ecology of bottlenose dolphins in the Kvarneric (Northern Adriatic Sea). Mar Mamm Sci 13:650–668

Booth CG, Sinclair RR, Harwood J (2020) Methods for monitoring for the population consequences of disturbance in marine mammals: a review. Front Mar Sci 7:115

Bradford AL, Weller DW, Punt AE, Ivashchenko YV, Burdin AM, VanBlaricom GR, Brownell RL Jr (2012) Leaner leviathans: body condition variation in a critically endangered whale population. J Mammal 93:251–266

Cartwright R, Venema A, Hernandez V, Wyels C, Cesere J, Cesere D (2019) Fluctuating reproductive rates in Hawaii's humpback whales, *Megaptera novaeangliae*, reflect recent climate anomalies in the North Pacific. R Soc Open Sci 6:181463

Cattet MRL, Caulkett NA, Obbard ME, Stenhouse GB (2002) A body-condition index for ursids. Can J Zool 80: 1156–1161

Cheeseman T, Barlow J, Acebes JM, Audley K and others (2024) Bellwethers of change: population modelling of North Pacific humpback whales from 2002 through 2021 reveals shift from recovery to climate response. R Soc Open Sci 11:231462

Chivers SJ, Baird RW, McSweeney DJ, Webster DL, Hedrick NM, Salinas JC (2007) Genetic variation and evidence for population structure in eastern North Pacific false killer whales (*Pseudorca crassidens*). Can J Zool 85:783–794

Chivers SJ, Baird RW, Martien KM, Taylor BL and others (2010) Evidence of genetic differentiation for Hawai'i insular false killer whales (*Pseudorca crassidens*). NOAA Tech Memo NMFS-SWFSC-458

Christiansen F, Dujon AM, Sprogis KR, Arnould JPY, Bejder L (2016) Noninvasive unmanned aerial vehicle provides estimates of the energetic cost of reproduction in humpback whales. Ecosphere 7:e01468

Christiansen F, Vivier F, Charlton C, Ward R, Amerson A, Burnell S, Bejder L (2018) Maternal body size and condition determine calf growth rates in southern right whales. Mar Ecol Prog Ser 592:267–281

Christiansen F, Sironi M, Moore MJ, Martino MD and others (2019) Estimating body mass of free-living whales using aerial photogrammetry and 3D volumetrics. Methods Ecol Evol 10:2034–2044

Christiansen F, Dawson SM, Durban JW, Fearnbach H and others (2020) Population comparison of right whale body condition reveals poor state of the North Atlantic right whale. Mar Ecol Prog Ser 640:1–16

Christiansen F, Rodríguez-González F, Martínez-Aguilar S, Urbán J and others (2021) Poor body condition associated with an unusual mortality event in gray whales. Mar Ecol Prog Ser 658:237–252

Christiansen F, Sprogis KR, Nielsen MLK, Glarou M, Bejder L (2023) Energy expenditure of southern right whales varies with body size, reproductive state and activity level. J Exp Biol 226:jeb245137

Christiansen F, Tervo OM, Heide-Jørgensen MP, Teilmann J (2024) Prey consumption of bowhead whales in West Greenland estimated from drone measurements of body size and condition. Polar Biol 47:17–39

Costa DP, Williams TM (1999) Marine mammal energetics. In: Reynolds JE, Rommel SA (eds) The biology of marine mammals. Smithsonian Institution Press, Washington, DC, p 176–217

Currie JJ, van Aswegen M, Stack SH, West KL, Vivier F, Bejder L (2021) Rapid weight loss in free ranging pygmy killer whales (*Feresa attenuata*) and the implications for anthropogenic disturbance of odontocetes. Sci Rep 11: 8181

Dawson SM, Bowman MH, Leunissen E, Sirguey P (2017) Inexpensive aerial photogrammetry for studies of whales and large marine animals. Front Mar Sci 4:366

Durban JW, Moore MJ, Chiang G, Hickmott LS and others (2016) Photogrammetry of blue whales with an unmanned hexacopter. Mar Mamm Sci 32:1510–1515

Durban JW, Fearnbach H, Paredes A, Hickmott LS, LeRoi DJ (2021) Size and body condition of sympatric killer whale ecotypes around the Antarctic Peninsula. Mar Ecol Prog Ser 677:209–217

Favilla AB, Adamczak SK, Costa DP (2024) Thermoregulation. In: Fahlman A, Hooker AK (eds) The physiology of dolphins. Academic Press, London, p 29–47

Ferreira IM (2008) Growth and reproduction in false killer whales (*Pseudorca crassidens* Owens, 1846). MSc thesis, University of Pretoria

Ferreira IM, Kasuya T, Marsh H, Best PB (2014) False killer whales (*Pseudorca crassidens*) from Japan and South Africa: differences in growth and reproduction. Mar Mamm Sci 30:64–84

Flament P (1996) Ocean atlas of Hawai'i. https://www.pacioos.hawaii.edu/education/ocean-atlas/#temperature

Foster EA, Franks DW, Morrell LJ, Balcomb KC, Parsons KM, van Ginneken A, Croft DP (2012) Social network correlates of food availability in an endangered population of killer whales, *Orcinus orca.* Anim Behav 83:731–736

Fox J (2019) An R companion to applied regression, 3rd edn. Sage Publications, Thousand Oaks, CA

Frankel AS, Gabriele CM, Yin S, Rickards SH (2022) Humpback whale abundance in Hawai'i: temporal trends and response to climatic drivers. Mar Mamm Sci 38:118–138

Gallagher CA, Chimienti M, Grimm V, Nabe-Nielsen J (2022) Energy-mediated responses to changing prey size and distribution in marine top predator movements and population dynamics. J Anim Ecol 91:241–254

Gilmartin M, Revelante N (1974) The 'island mass' effect on the phytoplankton and primary production of the Hawaiian Islands. J Exp Mar Biol Ecol 16:181–204

Glarou M, Gero S, Frantzis A, Brotons JM and others (2023) Estimating body mass of sperm whales from aerial photographs. Mar Mamm Sci 39:251–273

Gómez-Campos E, Borrell A, Correas J, Aguilar A (2015) Topographical variation in lipid content and morphological structure of the blubber in the striped dolphin. Sci Mar 79:189–197

Harnish AE, Baird RW, Mahaffy SD, Douglas AB and others (2024) False killer whales and fisheries in Hawaiian waters: evidence from mouthline and dorsal fin injuries reveal ongoing and repeated interactions. Endang Species Res 55:273–293

Hersh TA, Marcondes DS, Fonseca GF, Valle-Pereira JVS and others (2025) Ecology and conservation of socially learned foraging tactics in odontocetes. Philos Trans R Soc B 380:20240134

Kastelein RA, Mosterd J, Schooneman NM, Wiepkema PR (2000) Food consumption, growth, body dimensions, and respiration rates of captive false killer whales (*Pseudorca crassidens*). Aquat Mamm 26:33–44

Kastelein RA, Helder-Hoek L, Jennings N, van Kester R, Huisman R (2019) Reduction in body mass and blubber thickness of harbor porpoises (*Phocoena phocoena*) due to near-fasting for 24 hours in four seasons. Aquat Mamm 45:37–47

Keen KA, Beltran RS, Pirotta E, Costa DP (2021) Emerging themes in population consequences of disturbance models. Proc R Soc B 288:20210325

Koopman HN, Pabst DA, McLellan WA, Dillaman RM, Read AJ (2002) Changes in blubber distribution and morphology associated with starvation in the harbor porpoise (*Phocoena phocoena*): evidence for regional differences in blubber structure and function. Physiol Biochem Zool 75:498–512

Kotik C, Durban JW, Fearnbach H, Barrett-Lennard LG (2023) Morphometrics of mammal-eating killer whales from drone photogrammetry, with comparison to sympatric fish-eating killer whales in the eastern North Pacific. Mar Mamm Sci 39:42–58

Kratofil MA, Ylitalo GM, Mahaffy SD, West KL, Baird RW (2020) Life history and social structure as drivers of persistent organic pollutant levels and stable isotopes in Hawaiian false killer whales (*Pseudorca crassidens*). Sci Total Environ 733:138880

Kuczaj S (2010) Research with captive marine mammals is important: an introduction to the special issue. Int J Comp Psychol 23:225–226

Lundin JI, Ylitalo GM, Booth RK, Anulacion B and others (2016) Modulation in persistent organic pollutant concentration and profile by prey availability and reproductive status in southern resident killer whale scat samples. Environ Sci Technol 50:6506–6516

Mahaffy SD, Baird RW, Harnish AE, Cullins T and others (2023) Identifying social clusters of endangered main Hawaiian Islands false killer whales. Endang Species Res 51:249–268

Mann J, Connor RC, Barre LM, Heithaus MR (2000a) Female reproductive success in bottlenose dolphins (*Tursiops* sp.): life history, habitat, provisioning, and group-size effects. Behav Ecol 11:210–219

Mann J, Connor RC, Tyack PL, Whitehead H (eds) (2000b) Cetacean societies: field studies of dolphins and whales. University of Chicago Press, Chicago, IL

Martien KK, Chivers SJ, Baird RW, Archer FI and others (2014) Nuclear and mitochondrial patterns of population structure in North Pacific false killer whales (*Pseudorca crassidens*). J Hered 105:611–626

Merkle JA, Abrahms B, Armstrong JB, Sawyer H, Costa DP, Chalfoun AD (2022) Site fidelity as a maladaptive behavior in the Anthropocene. Front Ecol Environ 20:187–194

Napoli C, Hirtle N, Stepanuk J, Christiansen F and others (2024) Drone-based photogrammetry reveals differences in humpback whale body condition and mass across North Atlantic foraging grounds. Front Mar Sci 11:1336455

NMFS (National Marine Fisheries Service) (2012) Endangered status for the main Hawaiian Islands insular false killer whale distinct population segment. Fed Regis 77:70915–70939

NOAA Coral Reef Watch (2025) NOAA Coral Reef Watch version 3.1. Daily 5 km satellite regional virtual station time series data for Northwestern Hawaiian Islands 2018–2019

Oleson EM, Boggs CH, Forney KA, Hanson MB and others (2010) Status review of Hawaiian insular false killer whales (*Pseudorca crassidens*) under the Endangered Species Act. NOAA Tech Memo NMFS-PIFSC-22

Phipps JE, Silva-Krott I, Marchetti J, West KL (2023) Variation in blubber thickness and histology metrics across the body topography of a false killer whale (*Pseudorca crassidens*). Front Physiol 14:1001734

Pirotta E, Booth CG, Costa DP, Fleishman E and others (2018) Understanding the population consequences of disturbance. Ecol Evol 8:9934–9946

Pirotta E, Mangel M, Costa DP, Goldbogen J and others (2019) Anthropogenic disturbance in a changing environment: modelling lifetime reproductive success to predict the consequences of multiple stressors on a migratory population. Oikos 128:1340–1357

Pratchett MS, Munday PL, Wilson SK, Graham NAJ and others (2008) Effects of climate-induced coral bleaching on coral-reef fishes — ecological and economic consequences. Oceanogr Mar Biol Annu Rev 46:251–296

Pratchett MS, Hoey AS, Wilson SK, Messmer V and others (2011) Changes in biodiversity and functioning of reef fish assemblages following coral bleaching and coral loss. Diversity (Basel) 3:424–452

R Core Team (2025) R: a language and environment for statistical computing. R Foundation for Statistical Computing, Vienna

Raverty S, Leger JS, Noren DP, Huntington KB and others (2020) Pathology findings and correlation with body condition index in stranded killer whales (*Orcinus orca*) in the northeastern Pacific and Hawaii from 2004 to 2013. PLOS ONE 15:e0242505

Rojano-Doñate L, Teilmann J, Wisniewska DM, Jensen FH and others (2024) Low hunting costs in an expensive marine mammal predator. Sci Adv 10:eadj7132

Serres A, Lin W, Liu B, Chen S, Li S (2024) Skinny dolphins: Can poor body condition explain population decline in Indo-Pacific humpback dolphins (*Sousa Chinensis*)? Sci Total Environ 917:170401

Shirane Y, Mori F, Yamanaka M, Nakanishi M and others (2020) Development of a noninvasive photograph-based method for the evaluation of body condition in free-ranging brown bears. PeerJ 8:e9982

Shomura RS (1987) Hawaii's marine fishery resources: yesterday (1900) and today (1986). Southwest Fish Cent Admin Rep H-87-21

Sibert J, Hampton J, Kleiber P, Maunder M (2006) Biomass, size, and trophic status of top predators in the Pacific Ocean. Science 314:1773–1776

Silva I (2013) Short note: presence and distribution of Hawaiian false killer whales (*Pseudorca crassidens*) in Maui County waters: a historical perspective. Aquat Mamm 39:409–414

Stack SH, Currie JJ, McCordic JA, Olson GL (2019) Incidence of odontocetes with dorsal fin collapse in Maui Nui, Hawaii. Aquat Mamm 45:257–265

Stewart JD, Durban JW, Fearnbach H, Barrett-Lennard LG, Casler PK, Ward EJ, Dapp DR (2021a) Survival of the fattest: linking body condition to prey availability and survivorship of killer whales. Ecosphere 12:e03660

Stewart JD, Durban JW, Knowlton AR, Lynn MS and others (2021b) Decreasing body lengths in North Atlantic right whales. Curr Biol 31:3174–3179.e3

Strandberg U, Käkelä A, Lydersen C, Kovacs KM, Grahl-Nielsen O, Hyvärinen H, Käkelä R (2008) Stratification, composition, and function of marine mammal blubber: the ecology of fatty acids in marine mammals. Physiol Biochem Zool 81:473–485

Torres WI, Bierlich KC (2020) MorphoMetriX: a photogrammetric measurement GUI for morphometric analysis of megafauna. J Open Source Softw 5:1825

University of Hawai'i News (2021) False killer whale dietary first. https://www.hawaii.edu/news/2021/03/21/false-killer-whale-dietary-first/ (accessed 15 Sep 2025)

van Aswegen M, Szabo A, Currie JJ, Stack SH and others (2025a) Maternal investment, body condition and calf growth in humpback whales. J Physiol 603:551–578

van Aswegen M, Szabo A, Currie JJ, Stack SH and others (2025b) Age-specific body length, mass and energetic cost of growth in humpback whales. Mar Ecol Prog Ser 770:171–194

van Aswegen M, Szabo A, Currie JJ, Stack SH and others (2025c) Energetic cost of gestation and prenatal growth in humpback whales. J Physiol 603:529–550

Vivier F, Wells RS, Hill MC, Yano KM and others (2023) Quantifying the age structure of free-ranging delphinid populations: testing the accuracy of unoccupied aerial system photogrammetry. Ecol Evol 13:e10082

Warton DI, Wright IJ, Falster DS, Westoby M (2006) Bivariate line-fitting methods for allometry. Biol Rev Camb Philos Soc 81:259–291

Warton DI, Duursma RA, Falster DS, Taskinen S (2012) Smatr 3 — an R package for estimation and inference about allometric lines. Methods Ecol Evol 3:257–259

Wasser SK, Lundin JI, Ayres K, Seely E and others (2017) Population growth is limited by nutritional impacts on pregnancy success in endangered Southern Resident killer whales (*Orcinus orca*). PLOS ONE 12: e0179824

Williams TM, Davis RW (2024) Energetic costs of rest and locomotion in dolphins. In: Fahlman A, Hooker SK (eds) The physiology of dolphins. Academic Press, London, p 9–28

Williams TM, Haun J, Davis RW, Fuiman LA, Kohin S (2001) A killer appetite: metabolic consequences of carnivory in marine mammals. Comp Biochem Physiol A Mol Integr Physiol 129:785–796

Williams R, Vikingsson GA, Gislason A, Lockyer C, New L, Thomas L, Hammond PS (2013) Evidence for density-dependent changes in body condition and pregnancy rate of North Atlantic fin whales over four decades of varying environmental conditions. ICES J Mar Sci 70: 1273–1280

Winston M, Oliver T, Couch C, Donovan MK and others (2022) Coral taxonomy and local stressors drive bleaching prevalence across the Hawaiian Archipelago in 2019. PLOS ONE 17:e0269068

WPRFMC (Western Pacific Regional Fishery Management Council) (2022) Annual stock assessment and fishery evaluation report for the Pacific Pelagic Fisheries fishery ecosystem plan 2021. Western Pacific Regional Fishery Management Council, Honolulu, HI

Würsig B, Würsig M (1977) The photographic determination of group size, composition, and stability of coastal porpoises (*Tursiops truncatus*). Science 198: 755–756

Editorial responsibility: Jeremy Kiszka, North Miami, Florida, USA
Reviewed by: L. Fouda, M. A. Kratofil, J. R. Zaeschmar
Submitted: September 17, 2025; Accepted: March 11, 2026
Proofs received from author(s): May 30, 2026